

NASA Technical Memorandum 105632
AIAA-92-0691

Effect of Radiation on Convection at Moderate Temperatures

Henry C. deGroh III
Lewis Research Center
Cleveland, Ohio

and

Mohammad Kassemi
Ohio Aerospace Institute
Brook Park, Ohio

Prepared for the
30th Aerospace Sciences Meeting and Exhibit
sponsored by the American Institute of Aeronautics and Astronautics
Reno, Nevada, January 6-9, 1992

NASA

EFFECT OF RADIATION ON CONVECTION AT MODERATE TEMPERATURES

Henry C. deGroh III
National Aeronautics and Space Administration
NASA Lewis Research Center
Cleveland, Ohio 44135

Mohammad Kassemi*
Ohio Aerospace Institute
Brook Park, Ohio 44142

Abstract

The top-heated enclosure is of considerable importance in many engineering situations especially in crystal growth from vapor where it is used to minimize convection. In this work we present a combined numerical and experimental investigation of radiation induced convection to show that the convective stability of the top-heated enclosure is disrupted by heat transfer conditions at the wall. When the enclosure is not insulated the thermal stratification of the fluid is modified by convective and radiative losses to the surrounding environment. This results in a double annular cell flow which when cut by the laser sheet shows a four-vortex pattern with a weak annular cell at the bottom and a large counter-rotating annular cell at the top. When the enclosure is insulated the convective stability of the fluid is again disrupted; this time as a result of radiative heat transfer between the enclosing surfaces which drives two annular flow cells of relatively equal size. Comparison between model and experiment shows that radiation effects are important even at temperature levels as low as 300 °C and if these effects are not included, numerical predictions can be far removed from reality.

Introduction

Due to its widespread application in various engineering disciplines, natural convection in enclosures has received considerable attention in the past decade. A recent review by Ostrach¹ presents a comprehensive survey of the subject. It is apparent that in the majority of the problems considered to date, the contribution of radiation heat transfer is neglected. Nevertheless, there are many engineering applications such as fire research, combustion, and materials processing (e.g. crystal growth and glass forming) where radiation can strongly interact with convection and therefore affect both the temperature distributions and the flow fields (Yang²; Viskanta³).

The top-heated enclosure is often used in crystal growth from the vapor phase to eliminate convection. This orientation has also been used as a convenient means by which the diffusive flow regimes governing crystal growth in space can be simulated on earth. Previous numerical investigations of crystal growth in the top-heated orientation presented by Kassemi and Duval^{4,5} indicated that most of the nonuniformities in the growth flux are due to convection caused by radiation heat transfer. Such variations in the growth flux cause segregation, which is detrimental to crystal quality. The effects of radiation-influenced convection were also reported by Ross et al.⁶ in their numerical investigation of accidental fires (in both 1-g and low-g environments) caused by liquid fuel pools in the vicinity of a concentrated heat source. They numerically simulated the pre-ignition process in an enclosure with the heat source on top. Their results indicated an intricate flow pattern in the vapor-fuel mixture above the liquid fuel pool induced by radiation heat transfer, this detail was absent when radiation was neglected.

In recent years there have been numerous combined experimental and theoretical investigations of natural convection in enclosures. However, most of these studies have emphasized the effects of aspect ratio and inclination angle. One of the pioneering works in this area was conducted by Hart⁷ who used both experimental and analytical procedures to reveal significant

*NASA Resident Research Associate at Lewis Research Center.

features of enclosure inclination between two limiting cases; Bernard convection and convection in a vertical slot. This work was later extended in a series of papers by Ozoe et al.⁸⁻¹⁰ who carried out experimental and numerical studies of convection in inclined enclosures with different boundary conditions and aspect ratios. They provided valuable information concerning flow patterns, velocities and temperature distributions. The most recent combined experimental and numerical approach has been due to Hamady et al.¹¹ who again concentrated on the effect of inclination angle. The comprehensive comparison of the fluid motion and temperature contours visualized experimentally with the numerically predicted patterns of flow and isotherms presented in their work⁹ has added greatly to the physical understanding of the hydrodynamic and thermal boundary layer interactions at different angles of inclination.

All of the above mentioned studies, however, reflect situations in which the influence of thermal radiation and its interaction with natural convection is either absent or ignored. In this paper we present a combined experimental and numerical examination of radiation influenced convection. Because of its importance and relevance to crystal growth and flame spread we will focus our attention solely on the top heated enclosure. Hamady et al.¹¹ have shown that for this orientation, due to the existence of convection, the local values of the convective heat transfer are different from unity. They attribute this convection to the thermal boundary conditions on the walls. We will however show radiation causes the flow patterns in the enclosure to be quite different from those reported in their paper. In order to concentrate on the radiation-convection interactions we restrict ourselves to a controlled model experiment in which the interacting complications of crystal growth by vapor transport or flame spread above a liquid pool are absent. Through a combined numerical and experimental analysis of the problem we will show that convection-radiation interactions are important even at temperatures as low as 300°C and can result in a complete modification of temperature profiles and fluid flow patterns.

Mathematical Formulation

Figure 1 shows a schematic of the cylindrical test cell. The test cell consists of a cylindrical glass tube capped at the top and bottom ends by two copper plates. In accordance with the experimental conditions described in the next section, the top and bottom walls are kept at uniform temperatures T_h and T_c respectively. The cylindrical glass enclosure is assumed to be conducting in both the radial and axial directions. The physical properties of glass are assumed to be constant with temperature and are evaluated at the mean temperature. The cylindrical wall

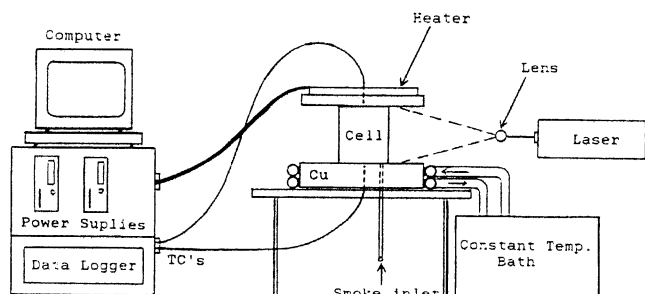


Figure 1. Experimental Set Up.

is subject to two types of boundary conditions. For the insulated case, it is subject to zero heat flux at the outer boundary of the wall and in the uninsulated case, it loses heat via radiation and convection to the outside environment. The working fluid is air. Because of the relatively large temperature difference between the top and bottom plates, air is modeled as a non-Boussinesq fluid. The thermo-physical properties of air are considered to be temperature dependant. Air is also assumed to be transparent and radiation exchange between the enclosing surfaces is considered to be diffuse gray.

Flow in the enclosure is described by the momentum equation which is written as

$$\rho \left[\frac{\partial \hat{u}}{\partial t} + \hat{u} \cdot \nabla \hat{u} \right] = -\nabla p + \rho \hat{g} + \nabla \cdot [\mu (\nabla \hat{u} + \nabla \hat{u}^T)] \quad (\text{EQ 1})$$

The density of the fluid is described by the following general expression

$$\rho = \rho_o [1 - \beta_T (T - T_o)]$$

in which β_T is an arbitrary function of temperature.

Equation (1) is subject to the nonslip boundary condition at all the enclosing surfaces. The main driving force for the flow is the buoyancy term which couples the momentum and energy equations. The energy equation for a transparent fluid is written as a balance between convection and conduction

$$\rho C_p \left[\frac{\partial T}{\partial t} + \hat{u} \cdot \nabla T \right] = \nabla \cdot (k \nabla T) \quad (\text{EQ 2})$$

Due to the conjugated heat transfer situation there is a coupling between the fluid and the wall energy equations. The latter is written as

$$\rho_w C_{p_w} \left[\frac{\partial T_w}{\partial t} \right] = \nabla \cdot (k_w \nabla T_w) \quad (\text{EQ 3})$$

For the cylindrical wall the inside boundary condition is determined by a balance between radiation, conduction, and convection:

$$\hat{n}_i \cdot k_w \nabla T_w = \hat{n}_i \cdot k \nabla T - q_w \quad (\text{EQ 4})$$

The net radiative flux in the above equation is described in terms of diffuse grey radiation exchange among the cylindrical wall and the top and bottom copper plates:

$$q_w = W_w - H_w \quad (\text{EQ 5})$$

$$W_w = \epsilon_w \sigma T_w^4 - (1 - \epsilon_w) H_w \quad (\text{EQ 6})$$

$$H_w = \iint_A W_w(r') K(r, r') dA \quad (\text{EQ 7})$$

The outside thermal boundary conditions are represented by either of two cases;

a) The insulated-wall case in which the flux at the boundary is set to zero:

$$\hat{n}_o \cdot k_w \nabla T = 0 \quad (\text{EQ 8})$$

b) The uninsulated case in which there is a balance between conduction convection and radiation at the outside surface:

$$\hat{n}_o \cdot k_w \nabla T = h_c (T_w - T_\infty) + \epsilon_w \sigma (T_w^4 - T_\infty^4) \quad (\text{EQ 9})$$

The convective loss to the surrounding is modeled using a heat transfer coefficient h_c which for natural convective flows over cylindrical bodies is written as

$$h_c = \frac{k}{L} \left[0.678 Ra^{1/4} \left(\frac{Pr}{0.952 + Pr} \right)^{1/4} \right] \quad (\text{EQ 10})$$

A modified version of the finite element code FIDAP was adopted for the numerical simulations. The axisymmetric model uses a 35 by 16 mesh. Further refinement of the mesh did not produce more accurate results and the 35 by 16 mesh was found adequate

especially since it provided good agreement with experimental results. All numerical predictions presented here correspond to steady state results.

Experimental Procedures

The experimental component of the investigation is described below in terms of the apparatus, system and thermal characterization, and the flow visualization experiments.

The Apparatus

Flow visualization experiments were performed in cylindrical borosilicate glass enclosures. Cigarette smoke was used as tracer particles, and a laser sheet was employed to illuminate the centerline of the cylinder. A schematic of the apparatus is shown in Fig. 2.

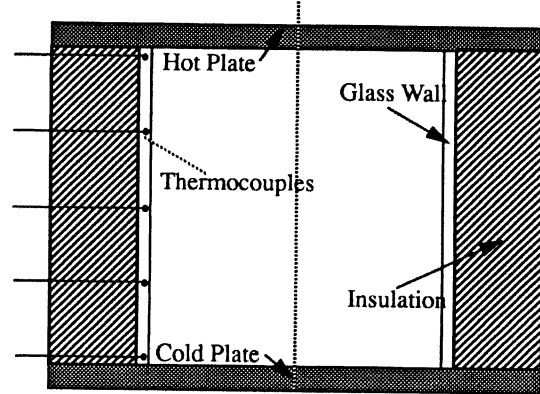


Figure 2. The Test Cell: Cylindrical Glass Enclosure.

The cylindrical test cells were constructed of borosilicate glass with a inner diameter and height of 40 mm and a wall thickness of about 2mm. The top and bottom walls of the cylinder were oxygen free high conductivity Cu disks with a diameter of 100mm. Both top and bottom Cu plates had a 3.8 mm deep groove into which the cylinder fit snugly. Contact between the glass and Cu ends was improved through use of a silver paste in the form of a partially dried and concentrated thread lubricant. This Silver Goop (Crawford Fitting Co. Solon, Ohio) was placed in the grooves of the Cu prior to test cell assembly. To maintain a known surface emittance, the Cu plates were coated with carbon (Spray Graph, American Resin & Chemical Corp., Wichita Falls, Texas). The emittance of the coated Cu ends was 0.62 ± 0.04 ¹².

The top plate was heated using a resistance heated disk with a diameter of 85 mm. The temperature of the bottom Cu plate, the cool end, was controlled using a constant temperature bath. The temperatures of the Cu ends were measured using fine thermocouples (36 gage Type K, 1mm dia. sheathing) inserted into the plates through small holes from the back sides of the cylinder ends and placed less than 1mm from the inside surface of the cylinder. These thermocouples gave temperature measurements within 0.4 °C of the surface temperature¹², not including the uncertainty of the thermocouple itself. Other studies of similar thermocouples have consistently shown an accuracy within 0.5 °C at 231.9 °C¹³. Thus the measurements of the inside surface temperatures of the Cu ends are believed to have an accuracy of approximately ± 1 °C. Power to the heater disk was delivered under computer control, using feed back from the Cu surface temperature measurement. Smoke was drawn into a 12 ml syringe and then put into the cylinder through 1mm dia. holes in the Cu bottom.

The centerline of the cylinder was illuminated by a laser sheet. The laser sheet was produced by placing a 6 mm dia. glass rod directly in front of a 1 milliwatt He-Ne laser (with a wavelength of

632.8 nm). More intense illumination was achieved by placing a first-surface-mirror on the side of the cylinder opposite the laser. The cylinder was placed in a 16 x 28 cm black box containing slits for the laser and a view port. This box helped to minimize glare on cylinder surfaces and forced convection from the laboratory's heating and air conditioning fans. This box may also have protected the test cell from the convective currents in the lab to some extent, effectively lowering the heat transfer coefficient for the uninsulated cases.

System and Thermal Characterization

Characterization of the test cell began with analysis of the top and bottom Cu plate temperatures. To detect undesired thermal gradients across the heated Cu, 19 thermocouples were soldered to the surface in a cross (+) pattern. Surface temperature measurements are difficult and very sensitive to the thermocouple contact. Therefore, the thermocouples were first calibrated by immersing the side of the copper plate opposite the thermocouples in boiling water and later in peanut oil (at 200 °C). These tests showed the temperature of the Cu plate constant to within 0.005 °C at 100 °C and 0.003 °C at 200 °C. Similar, temperature uniformity was assumed for the cooled Cu plate. The bath maintained temperatures to within 0.5 °C for the cool disk, as did the computer and power supplies for the heater disk.

In the top heated enclosure, the flow is basically driven by the radial temperature gradients set up by the temperature profiles of the side wall. Therefore accurate measurement of these profiles is important for the thermal characterization of the system. Temperature measurement along the sidewall were made for two different cases. In the first case the test cell was insulated from the environment by a jacket of 1" thick glass wool. In the second case the insulation was removed so that the test cell was exposed to the surrounding laboratory environment. In both cases the bottom Cu disk was kept at 30°C and the temperature difference between the ends was varied from 100 °C to 450 °C. However, for the sake of brevity this study will concentrate on temperature differences of 300 and 400 °C. The temperatures along the height of the cylinder were measured at five locations using thermocouples glued into 0.5mm holes in the glass, as shown in Fig. 2. The thermocouple tips were located at the inside edge of the test cell wall. Since surface temperature measurements are difficult and highly dependent on the thermocouple contact, the temperatures were also measured on the opposite side of the cylinder at the same height locations; all these temperature measurements were then repeated using a new cylinder, new thermocouples, fresh insulation, and a different type of glue to bond the thermocouples in the holes on the test cell wall. These repeated measurements yielded more accurate temperature profiles and helped to determine the uncertainties of the temperature measurements. Temperature measurements were stable after about 10 minute at a constant set-point temperature and did not vary significantly over time. When fully insulated, temperature measurements at the same height on opposite sides of the cylinder varied by about ± 3 °C at a hot plate temperature of 330 °C and ± 5 °C at 430 °C. During experiments with no insulation on the outside wall of the cylinder temperatures varied by as much as ± 6 °C on opposite sides.

The optical properties of the smoke were measured using a Perkin-Elmer 1750 Infrared Fourier Transform Spectrometer with a cell path length of 50mm. The smoke used was produced from Winston filtered cigarettes (R.J. Reynolds Tobacco Co., Winston-Salem, North Carolina). It was decided that the smoke and air mixture used in a typical visualization experiment can be assumed to be transparent to thermal radiation. The apparatus was calibrated using nitrogen gas and checked with air at the beginning and end of the smoke analysis experiments. Smoke was injected into the spectrometer test cell with the same 12ml syringe used in the flow experiments. An attempt was made to determine the variability of the smoke properties by injecting either one or

two syringes full of smoke into the test cell. It was found that one injection of smoke would completely fill the cylinder and that no difference in properties was detected.

Flow Visualization Experiments

In these experiments, end temperatures were set and maintained constant, smoke was injected into the cylinder and 35mm photographs were taken of the flow patterns. The size (cross-sectional area) and vortex location of the flow cells were then determined from the photographs. For all experiments the bottom surface of the cylinder was maintained at 30° C. The top surface of the cylinder was maintained at either 330° C or 430° C. The flow and temperature gradient along the cylinder were studied with the cylinder wall insulated and uninsulated. Therefore, in general four different cases were examined. End temperatures at the bottom and top were set and held constant for 20 minutes prior to introduction of smoke. In the insulated case, smoke was injected into the cylinder and after about 100 seconds, the insulation was quickly removed and the convective flow illuminated by the laser slice was photographed. In the uninsulated case, photographs were again taken about 100 seconds after input of smoke. In some cases it was found that flow cells could be better visualized by perturbing the flow (by quickly withdrawing a small amount of air from the inside of the cylinder) and then waiting about 15 seconds for the flow cells to reform and stabilize. The size, shape and location of the flow cells formed after perturbation were the same as those prior to the disturbance (within the uncertainties described below).

From the photographs, flow stream lines were drawn using an electromagnetic digitizer and vortex locations and flow cell sizes (cross-sectional area) were determined. Photographs from at least two different runs for each set of experimental conditions were analyzed. From these results approximate uncertainties were determined. Consequently, it is estimated that the vortex locations are accurate to within about $\pm 3\%$ relative to the ampoule radius of 2cm and flow cell area measurements are accurate to within about $\pm 3\%$ and $\pm 6\%$ for the top and bottom cells respectively. Vortex locations and cell sizes were also determined for the flow predicted by the model. Plots of the stream lines in conjunction with velocity vector plots were used to mark vortex locations and cell areas. Error associated with the limitations of the digitizer and the numerical predictions were determined to be approximately $\pm 1\%$ for the top and $\pm 4\%$ for the bottom cell vortex locations, and $\pm 2\%$ for the area measurements

Results

The first case considered is the insulated cylinder with the top plate kept at 330 °C and the bottom plate at 30 °C. In order to show the effect of radiation it is best to first present the numerical results obtained when radiation heat transfer is excluded from the model. The flow field for this case is shown in Fig. 3. In this case, conduction is the mode of heat transfer in both the air and glass wall. As a result, a linear temperature profile develops in the wall (see Fig. 4) and in the enclosure causing vertical stratification of the fluid. However, because the conductivity of air is different from that of glass, transverse temperature gradients are created in the enclosure. These transverse temperature differences are relatively small, but they are still sufficient to set up a very weak symmetrical recirculating flow in the enclosure with the cooled air sinking slowly near the wall (see Fig. 3) and the warmer air rising from the middle of the enclosure. While these predictions seem quite plausible, both the wall temperature distributions and the flow patterns are quite different from those observed experimentally. The experimental results for this case are presented in Figs. 4 and 5. Note that the wall temperature profile measured by the thermocouples is quite different from the ones predicted by the no-radiation model shown in Fig. 4. The flow patterns are also very different. The experimentally visualized flow indicates

a double annular cell pattern which when cut by the laser sheet is represented by four vortices. The fluid rises along the sidewall in the smaller bottom annulus and sinks near the sidewall in the top annulus.

When radiation heat transfer is included in the model, the predictions are significantly different from the no-radiation results. At a temperature of 330 °C, most of the radiation emitted by the heated copper plate is in the infrared wavelength region and is, therefore, totally absorbed by the glass wall¹⁴. As a result, the wall temperature distribution is significantly altered from the linear profile predicted previously. Due to the radiation emitted by the hot plate and absorbed by the glass, the temperature of the sidewall rises drastically, especially near the lower portion of the enclosure (the cold surface). Fig. 4 indicates an excellent agreement between the thermocouple measurements and the numerical results when radiation is included. This temperature distribution is the main driving force for the flow and results in a double annulus flow pattern depicted as four vortices in Fig. 6. The close correspondence between the experimental visualization results and the flow patterns predicted by the model is evident from a comparison between Figs. 5 and 6. Note that in both the model and the experiment the two bottom vortices are closer to the walls than the two top vortices. Table 1 shows a quantitative comparison of the cell sizes and locations. The model predicts the vortex location to within 10% of the experimental results and the cell sizes to within 5%.

In the insulated cylinder case, numerical predictions of the wall temperatures and flow patterns were also compared to experiments with the top plate kept at 430 °C. The experimental results for this case are included in Figs 7 and 8. A comparison between these results and those of the 330 °C case indicates that due to the increased radiative heat transfer, the temperature of the sidewall increases especially near the cold plate (see Fig. 7). Therefore, as the visualized flow patterns demonstrate (Fig. 8), the bottom annular cell becomes larger. The numerical results for this case are presented in Figs. 7 and 9. There is again excellent agreement between the predicted and measured wall temperatures, as shown in Fig. 7. A close comparison between the flow patterns in Fig. 9 and the 330 °C results indicates that the model also predicts that the bottom annulus grows larger as the temperature of the hot plate is increased to 430 °C. Table 1 indicates that the extent of the size increase observed experimentally is predicted by the model. These results clearly show that even in certain moderate temperature situations, radiative heat transfer has to be considered in the numerical models if reliable predictions are to be achieved.

The next case corresponds to the uninsulated cylinder in which the glass wall can lose heat via radiation and convection to the surrounding environment. The experimental wall temperature and flow patterns for the 330 °C case are presented in Figs. 10 and 11. It is apparent that the flow and wall temperature distributions in this case are significantly different from the previous insulated situation. Numerical predictions shown in Figs 10 and 12 also indicate this trend. In this case both the experiment and the model predict a small annular cell in the bottom of the enclosure and a large cell at the top. The model indicates that unlike the insulated case the two bottom vortices are much weaker than the top ones. A quantitative comparison between the cell sizes and locations is presented in Table 1 and again shows good agreement. However, the wall temperature profiles presented in Fig. 10 shows a larger discrepancy between the measured and computed values than for the previous insulated wall cases. We attribute this mainly to the fact that the convective heat transfer coefficient taken from the literature and used in the model does not exactly correspond to the flow patterns created around the cell by the complicated geometry of the apparatus.

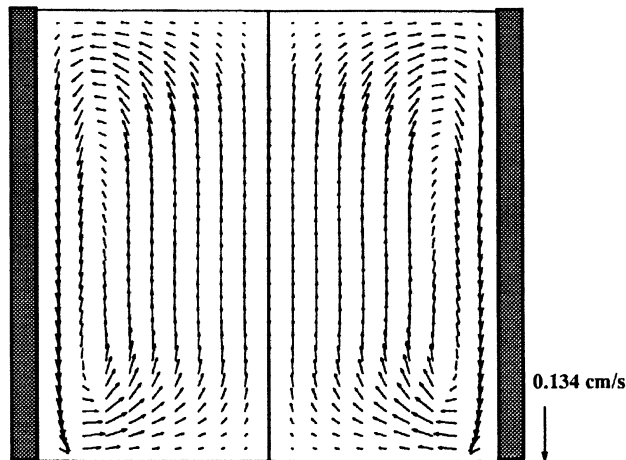


Figure 3. Predicted 2-D Vector Field Representing a Single Large Annulus inside The Insulated Cylinder with $T_h = 603$

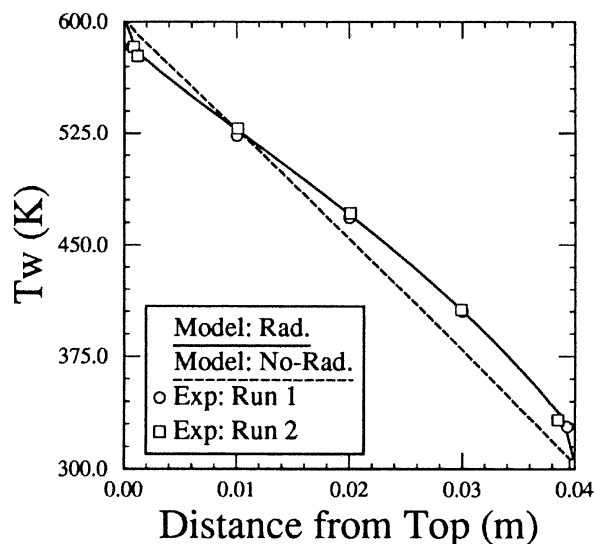


Figure 4. Wall Temperature Profile for the Insulated Case with $T_h = 603$ K; Dashed Line Excludes Radiation; Solid line Includes Radiation; Data Points Represent Temperature Measurements.

Table 1: Comparison of Vortex Location and Cell Sizes

	Insulated Enclosure				Uninsulated Enclosure			
	$T_h = 330$ °C		$T_h = 430$ °C		$T_h = 330$ °C		$T_h = 430$ °C	
Vortex Location (x,y) cm	Experiment	Model	Experiment	Model	Experiment	Model	Experiment	Model
Top Cell	1.45, 3.12	1.25, 2.86	1.43, 3.08	1.21, 2.85	1.55, 2.96	1.39, 2.73	1.51, 2.92	1.39, 2.85
Bottom Cell	1.72, 0.49	1.43, 0.59	1.69, 0.50	1.40, 0.64	1.76, 0.39	1.52, 0.44	1.79, 0.40	1.52, 0.55
Vortex Size cm ²	Experiment	Model	Experiment	Model	Experiment	Model	Experiment	Model
Top Cell	5.20	5.08	4.64	4.69	6.15	6.48	5.79	5.66
Bottom Cell	2.80	2.92	3.36	3.31	1.85	1.52	2.21	2.34

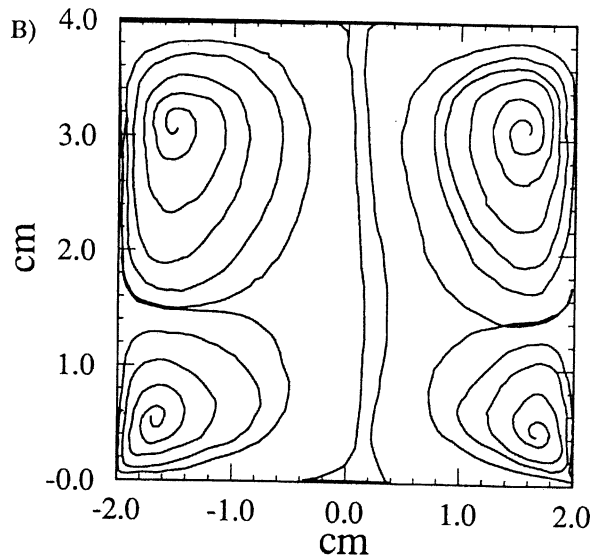
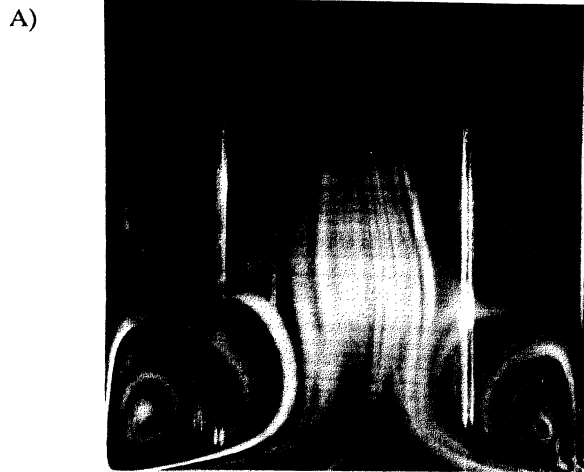


Figure 5. Experimental Results for The Insulated Cylinder with $T_h = 603$ K; a) Visualized Flow Patterns; b) Digitized Flow Patterns.

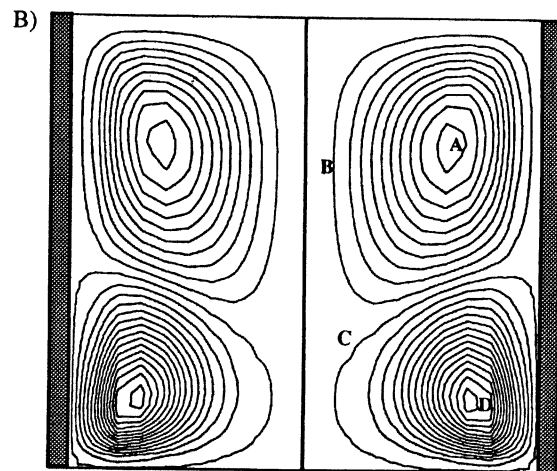
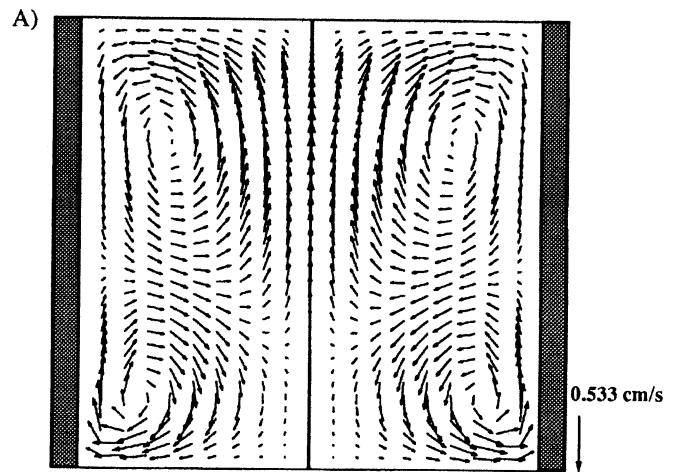


Figure 6. Predicted Flow Patterns Showing Upper and Lower Annuli for The Insulated Cylinder with $T_h = 603$ K; a) Vector Field; b) Streamlines, $A = 0.8382(10^{-6})$, $B = 0.6928(10^{-7})$, $C = 0.1616(10^{-7})$, $D = 0.1212(10^{-5})$.

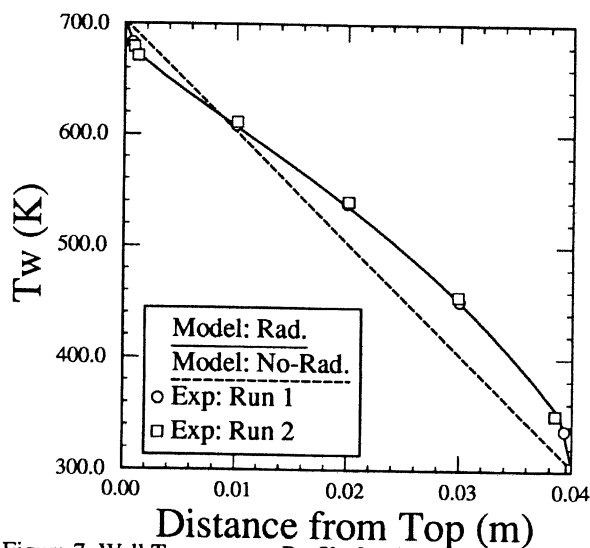


Figure 7. Wall Temperature Profile for the Insulated Case with $T_h = 703$ K; Dashed Line Excludes Radiation; Solid line Includes Radiation; Data Points Represent Temperature Measurements.

When the temperature of the hot plate in the uninsulated case is changed to 430 °C, we observe an increase in the size of the bottom cells. This is reflected in Fig. 13 and 14 and Table 1. There is still a significant discrepancy between the measured and predicted wall temperatures as shown in Fig. 15. But again the close correspondence achieved between the flow patterns predicted by the model and the ones observed experimentally seem to be unaffected by these discrepancies.

Conclusions

In this work we have presented a combined numerical and experimental investigation of radiation induced convection in the top-heated enclosure; an orientation which is of considerable importance in many engineering situations especially in crystal growth from vapor. A modified version of FIDAP accurately predicted the number and direction of the flow cells. Flow cell sizes and vortex locations were numerically determined to within 5% and 10% of experimental values respectively. Our results show that the convective stability of the top-heated enclosure is disrupted by heat transfer conditions at the wall. When the enclosure is not insulated the thermal stratification of the fluid is modified by convective and radiative losses to the surrounding environment and internal surface radiation exchange. This results in a double annular cell pattern with two extremely weak vortices in the bot-

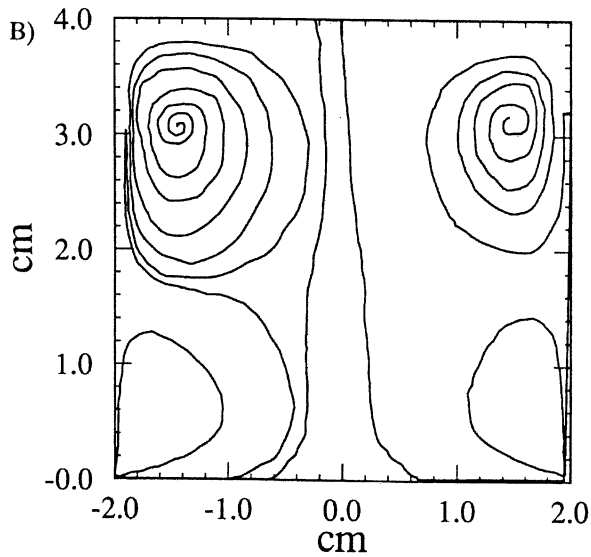
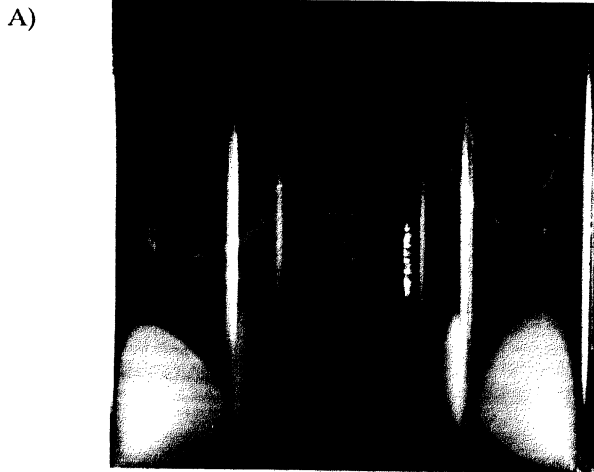


Figure 8. Experimental Results for The Insulated Cylinder with $T_h = 703$ K; a) Visualized Flow Patterns; b) Digitized Flow Patterns.

tom and two large counter-rotating vortices at the top. When the enclosure is insulated the convective stability of the fluid is again disrupted; this time solely due to radiative heat transfer between the enclosing surfaces which drives two annuli of relatively equal size. Comparison between models and experiment suggests that radiation effects are important even at temperature levels as low as 300°C . If the effect of radiation heat transfer are not included numerical predictions can be far removed from reality. Finally, as far as crystal growth experiments are concerned, it can be generalized that convective stable conditions cannot be achieved on earth even in the top heated orientation and in simple cylindrical enclosures, the diffusive flows desired by crystal growers may be possible only in the microgravity environment of space.

Nomenclature

A	Surface area
C_p	Heat Capacity
D	Diameter of the enclosure
g	Gravitational vector
H	Incident radiation flux
h_c	Coefficient of convective heat transfer
k	Thermal Conductivity
L	Length of the enclosure

(continued)

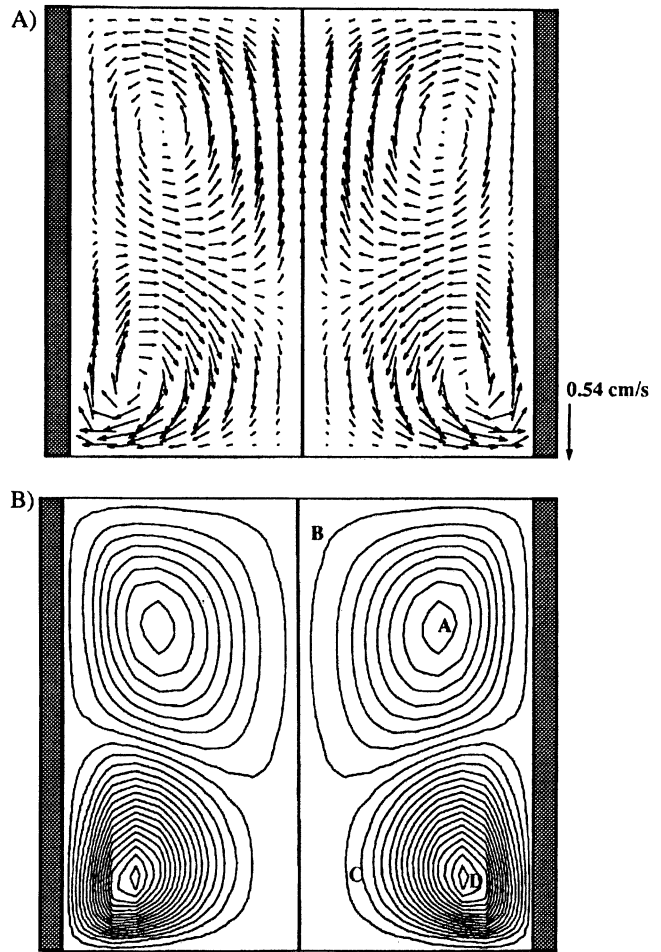


Figure 9. Predicted Flow Patterns Showing Upper and Lower Annuli for The Insulated Cylinder with $T_h = 703$ K; a) Vector Field; b) Streamlines, $A = -0.6300(10^{-6})$, $B = -0.2051(10^{-7})$, $C = 0.1536(10^{-6})$, $D = 0.1460(10^{-5})$.

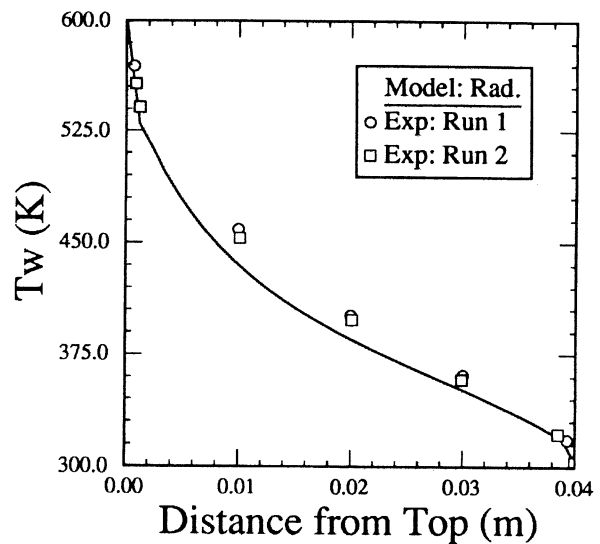


Figure 10. Wall Temperature Profile for the Uninsulated Case with $T_h = 603$ K; Solid line Represents Numerical Prediction; Data Points Represent Temperature Measurements.

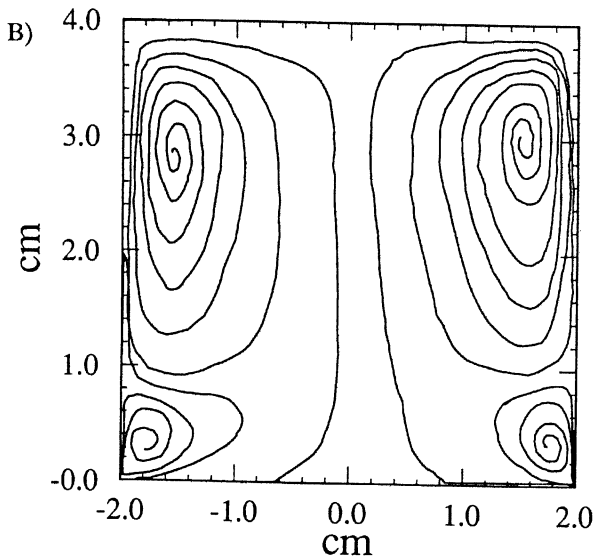
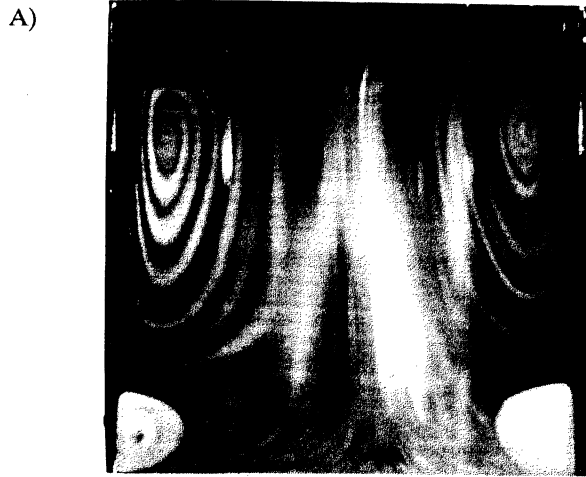


Figure 11. Experimental Results for The Uninsulated Cylinder with $T_h = 603$ K; a) Visualized Flow Patterns; b) Digitized Flow Patterns.

n_i	Unit normal vector (inside)
n_o	Unit normal vector (outside)
p	Pressure
Pr	Prandtl number
r	Radial coordinate
Ra	Raleigh number
T	Temperature
u	Velocity vector
W	Surface radiosity
x	Axial coordinate
Greek	
β_T	Coefficient of thermal expansion
ϵ	Surface emissivity
μ	Dynamic viscosity
ρ	Density
σ	Boltzmann constant
Subscripts	
c	Pertaining to the cold plate
o	Reference values
h	Pertaining to the hot plate
w	Pertaining to the walls
∞	Pertaining to the surrounding

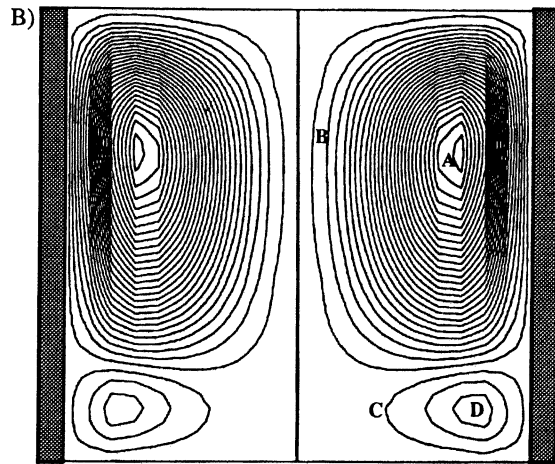
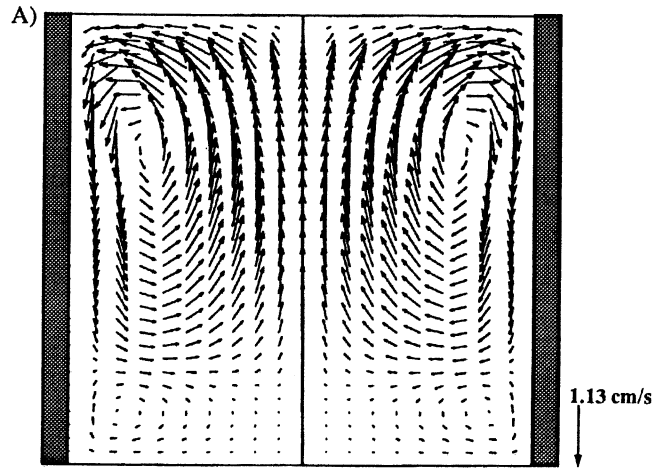


Figure 12. Predicted Flow Patterns Showing Upper and Lower Annuli for The Uninsulated Cylinder with $T_h = 603$ K; a) Vector Field; b) Streamlines, $A = -0.3283(10^{-3})$, $B = 0.6572(10^7)$, $C = 0.5803(10^{-7})$, $D = 0.3055(10^{-6})$.

Acknowledgment

The authors wish to gratefully acknowledge the helpful assistance and discussions provided by Dr. Christophe Mennetrier and Dr. Howard Ross.

References

- Ostrach, S., "Natural Convection in Enclosures," *Journal of Heat Transfer*, Vol. 110, 1988, p. 1175.
- Yang, K.T. "Numerical Modeling of Natural Convection-Radiation Interactions in Enclosures," *Heat Transfer 1986*, Hemisphere Publication, Vol. 1, 1986, p. 131.
- Viskanta, R., "Radiation Heat Transfer: Interaction with Conduction and Convection and Approximate Methods in Radiation," *Heat Transfer 1982*, Hemisphere Publication, Vol. 1, 1982, p. 103.
- Kassem, M. and Duval, W. "Effect of Gas and Surface Radiation on Crystal Growth from The Vapor Phase," *J. Physico-Chemical Hydrodynamics*, Vol. 11, 1989, p. 516.
- Kassem, M. and Duval, W. "Interaction of Surface Radiation with Convection in Crystal Growth by Vapor Transport," *Journal of Thermophysics and Heat Transfer*, 1990, p. 454.

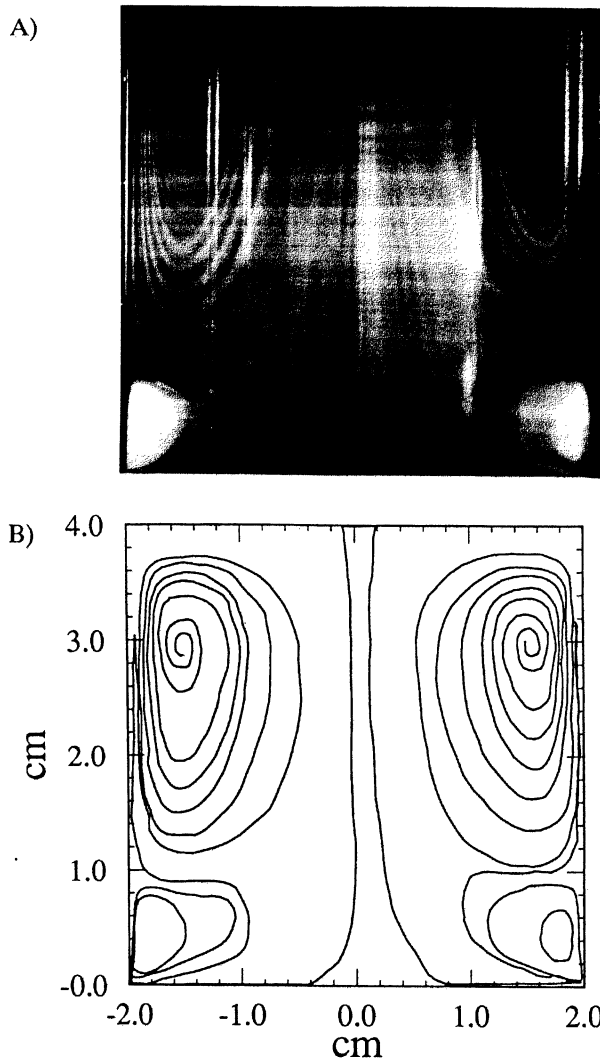


Figure 13. Experimental Results for The Uninsulated Cylinder with $T_h = 703$ K; a) Visualized Flow Patterns; b) Digitized Flow Patterns.

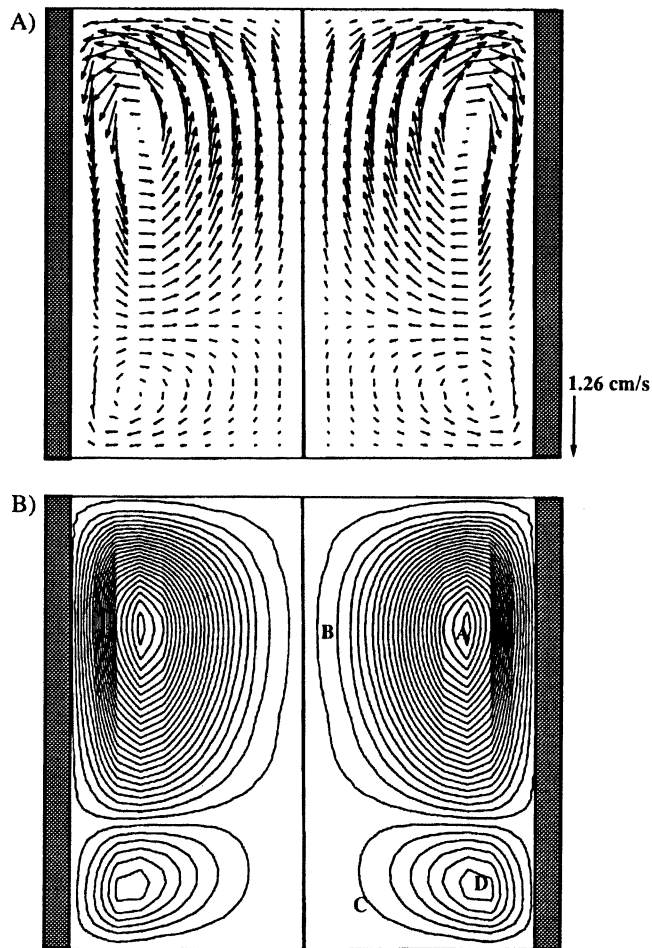


Figure 14. Predicted Flow Patterns Showing Upper and Lower Annuli for The Uninsulated Cylinder with $T_h = 703$ K; a) Vector Field; b) Streamlines, $A = -0.3107(10^{-5})$, $B = -0.4355(10^{-7})$, $C = 0.8963(10^{-7})$, $D = 0.7556(10^{-6})$.

6. Ross, H.D. et al. (1989) "Behavior in Normal and Reduced Gravity of an Enclosed Liquid/Gas System with Nonuniform Heating From Above," *AIAA paper 89-0070*, presented in the 27th Aerospace Sciences Meeting, Reno Nevada, 1989.
7. Hart, J.E., "Stability of The Flow in a Differentially Heated Inclined Box," *J. Fluid Mechanics*, Vol. 47, 1971, pp. 547-576.
8. Ozoe, H., Sayama, H., and Churchill, W., "Natural Convection in an Inclined Square Channel at Various Aspect Ratios and Angles - Experimental Measurements," *Int. J. Heat Mass Transfer*, Vol. 18, 1975, pp. 1425-1431.
9. Ozoe, H., Sayama, H., and Churchill, W., "Natural Convection in an Inclined Square Channel," *Int. J. Heat Mass Transfer*, Vol. 17, 1974, pp. 401-406.
10. Ozoe, H., Fuji, K., Lior, N., and Churchill, W., "Long Rolls Generated by Natural Convection in an Inclined Rectangular Enclosure," *Int. J. Heat Mass Transfer*, Vol. 26, 1983, pp. 1427-1438.
11. Hamady, F.J., Lloyd J.R., Yang, H.Q. and Yang K.T., "Study of Local Natural Convection Heat Transfer in an Inclined Enclosure," *Int. J. Heat Mass Transfer*, Vol. 32, 1989, pp. 1697- 1707.

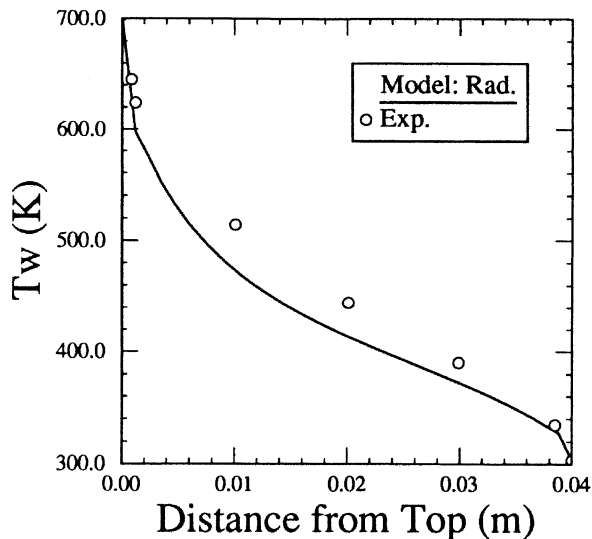


Figure 15. Wall Temperature Profile for the Uninsulated Case with $T_h = 703$ K; Solid line Represents Numerical Prediction; Data Points Represent Temperature Measurements.

12. de Groh, H.C. "Macroseggregation and Nucleation in Under-cooled Pb-Sn Alloys," Masters Thesis, Case Western Reserve University, Cleveland Ohio, 1989, also *NASA TM 102023*, May 1989.
13. Jackson, T.I., "A Study of the use of Surface Coatings to Improve the Accuracy of Radiation Temperature Measurements," Masters Thesis, Ohio State University, 1979
14. Holland, L.R., A Thermal Transmission Function For Fused Silica Ampoules, *J. Crystal Growth*, Vol 49, p 426.

REPORT DOCUMENTATION PAGE

Form Approved
OMB No. 0704-0188

Public reporting burden for this collection of information is estimated to average 1 hour per response, including the time for reviewing instructions, searching existing data sources, gathering and maintaining the data needed, and completing and reviewing the collection of information. Send comments regarding this burden estimate or any other aspect of this collection of information, including suggestions for reducing this burden, to Washington Headquarters Services, Directorate for Information Operations and Reports, 1215 Jefferson Davis Highway, Suite 1204, Arlington, VA 22202-4302, and to the Office of Management and Budget, Paperwork Reduction Project (0704-0188), Washington, DC 20503.

1. AGENCY USE ONLY <i>(Leave blank)</i>	2. REPORT DATE January 1992	3. REPORT TYPE AND DATES COVERED Technical Memorandum	
4. TITLE AND SUBTITLE Effect of Radiation on Convection at Moderate Temperatures		5. FUNDING NUMBERS WU-674-21-05-00	
6. AUTHOR(S) Henry C. deGroh III and Mohammad Kassemi			
7. PERFORMING ORGANIZATION NAME(S) AND ADDRESS(ES) National Aeronautics and Space Administration Lewis Research Center Cleveland, Ohio 44135-3191		8. PERFORMING ORGANIZATION REPORT NUMBER E-6975	
9. SPONSORING/MONITORING AGENCY NAME(S) AND ADDRESS(ES) National Aeronautics and Space Administration Washington, DC 20546-0001		10. SPONSORING/MONITORING AGENCY REPORT NUMBER NASA TM-105632 AIAA-92-0691	
11. SUPPLEMENTARY NOTES Prepared for the 30th Aerospace Sciences Meeting and Exhibit sponsored by the American Institute of Aeronautics and Astronautics, Reno, Nevada, January 6-9, 1992. Henry C. deGroh III, NASA Lewis Research Center, Mohammad Kassemi, Ohio Aerospace Institute, 2001 Aerospace Parkway, Brook Park, Ohio 44142 and NASA Resident Research Associate at Lewis Research Center. Responsible person, Henry C. deGroh III, (216) 433-5025.			
12a. DISTRIBUTION/AVAILABILITY STATEMENT Unclassified - Unlimited Subject Category 34 This publication is available from the NASA Center for AeroSpace Information, (301) 621-0390.		12b. DISTRIBUTION CODE	
13. ABSTRACT <i>(Maximum 200 words)</i> The top-heated enclosure is of considerable importance in many engineering situations especially in crystal growth from vapor where it is used to minimize convection. In this work we present a combined numerical and experimental investigation of radiation induced convection to show that the convective stability of the top-heated enclosure is disrupted by heat transfer conditions at the wall. When the enclosure is not insulated the thermal stratification of the fluid is modified by convective and radiative losses to the surrounding environment. This results in a double annular cell flow which when cut by the laser sheet shows a four-vortex pattern with a weak annular cell at the bottom and a large counter-rotating annular cell at the top. When the enclosure is insulated the convective stability of the fluid is again disrupted; this time as a result of radiative heat transfer between the enclosing surfaces which drives two annular flow cells of relatively equal size. Comparison between model and experiment shows that radiation effects are important even at temperature levels as low as 300 °C and if these effects are not included, numerical predictions can be far removed from reality.			
14. SUBJECT TERMS Radiation; Convection; Crystal growth; Physical vapor transport			15. NUMBER OF PAGES 10
			16. PRICE CODE A02
17. SECURITY CLASSIFICATION OF REPORT Unclassified	18. SECURITY CLASSIFICATION OF THIS PAGE Unclassified	19. SECURITY CLASSIFICATION OF ABSTRACT Unclassified	20. LIMITATION OF ABSTRACT